OPEN

NPG Asia Materials (2017) 9, e408; doi:10.1038/am.2017.117
www.nature.com/am

ORIGINAL ARTICLE

In vivo targeted therapy of gastric tumors via the mechanical rotation of a flower-like Fe_3O_4@Au nanoprobe under an alternating magnetic field

Ting Yin[1], Haigang Wu[2], Qian Zhang[1], Guo Gao[1], Joseph G Shapter[3], Yulan Shen[4], Qiaozhi He[1], Peng Huang[1], Wen Qi[1], Chunlei Zhang[1], Yuming Yang[1] and Daxiang Cui[1]

Owing to their hypotoxicity, great spatial resolution and tomographic properties, Fe_3O_4 nanoparticles (NPs) are becoming one of the most promising materials for noninvasive biological imaging and shape-dependent therapeutic agents for malignant tumor therapy. Conventional spherical NPs are unable to effectively destroy cellular structure in therapy and thus result in tumors with a high risk of drug resistance. Herein we developed a novel flower-like targeting Fe_3O_4@Au-HPG-Glc nanoprobe (thiol-containing hyperbranched polyglycerol (HPG); 4-aminophenyl β-D-glucopyranoside (Glc)) that can enhance magnetic resonance imaging (MRI) for cancer therapy. With the guidance of a targeting molecule, Fe_3O_4@Au-HPG-Glc nanoprobes can precisely target tumor cells. Under an alternating magnetic field (AMF), the flower-like Fe_3O_4@Au-HPG-Glc nanoprobes can rotate along the central axis of the core to substantially destroy tumor cells by damaging the nucleus or cell membrane. Our results showed that this shape-dependent therapeutic agent-based strategy had remarkable efficacy for MRI-guided tumor therapy. Furthermore, the inhibition of tumor growth in tumor-bearing mice was up to approximately 47.3% on the twelfth day of treatment compared with the level of inhibition in a blank group. Different from other reported methods for cancer therapy, our proposed AMF-dependent targeted cancer therapy is a novel strategy that can potentially reduce drug resistance in gastric tumors.
NPG Asia Materials (2017) **9,** e408; doi:10.1038/am.2017.117; published online 14 July 2017

INTRODUCTION

With the development of advanced nanotechnology, the rational integration of multifunctional nanoplatforms for early diagnoses and cancer therapies are of great interest.[1,2] Among the imaging techniques, magnetic resonance imaging (MRI) is considered one of the most promising noninvasive clinical tools due to significant merits, such as excellent spatial resolution and sensitivity, and especially for providing excellent three-dimensional and tomographic contrast information of soft tissue.[3,4] The inherent characteristics of pure Fe_3O_4 nanoparticles (NPs; for example, poor colloidal stability and low targeted retention at the tumor site) have hindered their wide application in nanomedicine. Hence, surface modifications (for example, organic or inorganic coating) of pure Fe_3O_4 NPs have attracted extensive attention.[5,6] Fe_3O_4 NPs with modified surface layers have been used as carriers to deliver anticarcinogens.[7] Despite great efforts to explore anticancer adjuvants, the issue of drug resistance in cancer therapy remains a challenging problem. Herein we developed an oriented growth method for the controllable synthesis of flower-like Fe_3O_4@Au NPs. Owing to the axial dissymmetry of the flower-like Fe_3O_4@Au NPs, this nanoplatform freely rotates under an alternating magnetic field (AMF), which can efficiently destroy tumor cells. The unique properties of flower-like Fe_3O_4@Au NPs were superior to that of traditional spherical Fe_3O_4 magnetic NPs with symmetric structures.[8] The special structural property of flower-like Fe_3O_4 NPs allowed for the development of a high-efficiency MRI-guided therapy.

To improve the colloidal stability of Fe_3O_4@Au NPs, thiol-containing hyperbranched polyglycerol (HPG) with rich branches were bonded onto the surface of Fe_3O_4@Au NPs. The functional groups on the surfaces of the dendrimers enable the coupling of targeting ligands and fluorescent probes to be used as drug carriers for the diagnosis and therapeutic treatment of cancer.[9–11] Furthermore, these functional groups also act as excellent stabilizers or templates in the preparation of versatile nanoplatforms for biological imaging applications.[12–14] Modified NPs using HPG dendrimers have been shown to reduce the *in vivo* adsorption of plasma proteins on the polymer surfaces of NPs with diameters <100 nm.[15] Recently, efforts have focused on the application of biological targeting molecules (for

[1]Institute of Nano Biomedicine and Engineering, Shanghai Engineering Research Center for Intelligent Diagnosis and Treatment Instrument, Department of Instrument Science and Engineering, School of Electronic Information and Electrical Engineering, Shanghai Jiao Tong University, Shanghai, China; [2]School of Biomedical Engineering, Shanghai Jiao Tong University, Shanghai, China; [3]School of Chemical and Physical Sciences, Flinders University, Adelaide, SA, Australia and [4]Department of Radiology, Shanghai Jiao Tong University Affiliated Sixth People's Hospital, Shanghai Jiao Tong University, Shanghai, China
Correspondence: Professor G Gao and Professor D Cui, Institute of Nano Biomedicine and Engineering, Shanghai Engineering Research Center for Intelligent Diagnosis and Treatment Instrument, Department of Instrument Science and Engineering, School of Electronic Information and Electrical Engineering, Shanghai Jiao Tong University, Shanghai 200240, China.
E-mail: guogao@sjtu.edu.cn or dxcui@sjtu.edu.cn
Received 27 January 2017; revised 29 April 2017; accepted 12 May 2017

example, antibodies, carbohydrates and peptides) to modify the surface of nanoplatforms in biological systems.[16,17] Glucose is a carbohydrate and is an important energy source for cell survival and recognition.[18] Owing to high energy demands and metabolism in malignant cells, the cellular uptake of glucose varies among different cancer cell types.[19] In our previous work, we found that Au nanoprisms coated with glucose can effectively promote cellular uptake in gastric cancer for potential *in vivo* applications in imaging and therapy.[20,21] However, we noticed that traditional spherical nanoprobes face drug resistance issues in cancer therapy. Destroying malignant cellular structure has become one of the most effective ways to reduce drug resistance.

In this study, novel flower-like Fe_3O_4@Au-HPG-Glc nanoprobes were developed. One of the glucose derivatives, namely, 4-aminophenyl β-D-glucopyranoside (Glc), was used as the targeting molecule. These nanoprobes were designed to destroy malignant cellular structure by mechanically rotating the nanoprobes around the central axis of the core under an AMF. With the guidance of a targeting Glc molecule, the synthesized Fe_3O_4@Au-HPG-Glc nanoprobes precisely targeted tumor cells for MRI-guided therapy. Negatively charged gold clusters were loaded onto the surfaces of positively charged Fe_3O_4 NPs using electrostatic interactions and surface effects. The Fe_3O_4@Au NPs were modified with thiolated HPG dendrimers (SH-HPG) through S-Au bonds. HPG dendrimer terminals were coupled with Glc via acetylation. The synthesized flower-like Fe_3O_4@Au-HPG-Glc nanoprobes were applied as a T_2 contrast agent to trace the variations in tumors before and after treatment based on prolonged retention time and enhanced cellular uptake in the targeted region (Figure 1). The flower-like Fe_3O_4@Au-HPG-Glc nanoprobes were successfully applied in imaging-guided targeting cancer therapy under an AMF. The AMF-dependent therapy strategy can destroy the tumor cellular structure and reduce drug resistance.

EXPERIMENTAL PROCEDURES

Materials

Ethylene glycol, diethylene glycol, polyvinylpyrrolidone K30 (PVP), ferric chloride hexahydrate ($FeCl_3{\cdot}6H_2O$), sodium acetate trihydrate, ethanol, tetrahydrofuran, acetic acid, formaldehyde, hydrogen tetrachloroaurate (III) hydrate ($HAuCl_4{\cdot}4H_2O$), sodium borate ($Na_2B_4O_7{\cdot}10H_2O$), NaH (60% in mineral oil), bis(2-hydroxyethyl)disulfide and a dioxane solution of glycidol were purchased from the Sinopharm Chemical Reagent Co., Ltd. (Shanghai, China). Glutathione, Glc, *N*-hydroxysulfosuccinimide, 3-hydroxytyramine hydrochloride, 3-[4,5-dimethylthiazol-2-yl]-2 and 5-diphenyltetrazolium bromide (MTT), 1-ethyl-3-[3-dimethylaminopropyl] carbodiimide hydrochloride were obtained from Sigma-Aldrich Chemical Co., Ltd. (St Louis, MO, USA). MGC-803 cells were obtained from the Chinese Academy of Sciences, Beijing, China. All cell culture media were provided by GIBCO (Shanghai, China). Water was purified on a Milli-Q water system (Millipore Co., Bedford, MA, USA) with a resistivity of 18.2 MΩ at each step.

Preparation of flower-like Fe_3O_4@Au-HPG-Glc NPs

Synthesis of flower-like superparamagnetic Fe_3O_4 NPs. In a typical procedure, $FeCl_3{\cdot}6H_2O$ (8 mmol) was dissolved in a mixture of ethylene glycol and diethylene glycol (volume ratio of 3:17) under ultrasonic conditions at room temperature. After half an hour, 8 g of PVP was poured into the yellow transparent mixture under a nitrogen atmosphere and heated for 1 h at 125 °C. After the PVP surfactant was completely dissolved, NaOAc (6 g) was added, and the stirring speed was increased. After 0.5 h, the mixture was heated to 200 °C for 12 h in a 100-ml Teflon-lined stainless-steel autoclave. After reacting, Fe_3O_4 NPs were collected by magnetic separation and washed with ultrapure water (UPW) and ethanol three times. Then the obtained product was redispersed in the same volume of cold tetrahydrofuran. The synthesized Fe_3O_4 dispersion solution was stored in a freezer at 4 °C until required.

Synthesis of flower-like superparamagnetic Fe_3O_4@Au NPs

Dopamine (DA) modification. Briefly, 20 mg of DA was dissolved in 1.5 ml UPW and added to a 5 ml Fe_3O_4 NP dispersion, which was sonicated for 1 h. The mixture was left on the shaking table overnight. The obtained Fe_3O_4-DA was purified via magnetic separation and well dispersed in 20 ml of UPW by ultrasound.

Gold seed. Red-emitting gold nanoclusters were used as gold seeds and prepared using previously reported procedures.[22] In a typical synthesis, $HAuCl_4$ (50 μmol) and glutathione (150 μmol) were mixed in a 100-ml round bottom flask with 50 ml of UPW. After reacting for 3 min, 3 ml of tetrabutylammonium bromide solution was poured into the mixture, and the solution was reacted for 5 min. The mixture was kept in an ice bath for 2 h, and 1 M HCl was added dropwise to adjust the pH to 3.0. Subsequently, the reaction solution

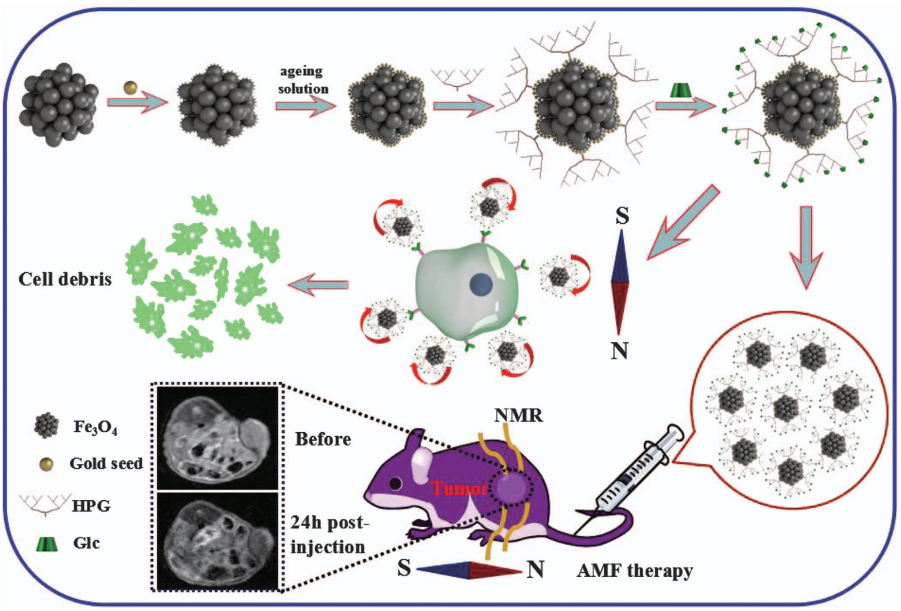

Figure 1 Schematic of flower-like Fe_3O_4@Au-HPG-Glc nanoprobes for *in vitro/vivo* MRI and therapy of gastric tumors under an alternating magnetic field.

was left to stand in an ice bath overnight. Negatively charged colloidal gold seeds were obtained.

Growth solution. $HAuCl_4$ (1.5 ml, 25 mM) was mixed into a 0.18 M potassium carbonate solution. After stirring for 10 min, the faint yellow solution turned colorless. After another 24 h, the growth solution was formed and stored in a fridge at 4 °C for future experiments.

Fe_3O_4@Au NPs. First, the negatively charged red-emitting gold nanoclusters were attached to the surface of the DA-modified Fe_3O_4 NPs through electrostatic interactions. The red-emitting gold nanoclusters (200 μl, 12 mg ml^{-1}) were added to 2 ml of Fe_3O_4-DA. Subsequently, 5 ml of UPW was quickly added, and the mixture was shaken for 5 min. Then 0.2 M acetic acid solution was added dropwise into the mixture to adjust the pH to ~4.0. The reaction solution was shaken for 12 h and purified using magnetic separation three times. The collected Fe_3O_4@Au seed NPs were dissolved in 5 ml of UPW. Subsequently, a dense gold shell on the surface of Fe_3O_4 NPs was formed by a seed-induced growth method. Then 10 ml of this gold growth solution was poured into the Fe_3O_4@Au seed-dispersing agent (5 ml) under vigorous shaking. Formaldehyde solution (6 ml, volume ratio of formaldehyde to UPW of 1:1), acting as a reducing agent, was added to the reaction mixture dropwise. Then the mixture was vigorously shaken for another 30 min. Thus the gold NPs were loaded onto the Fe_3O_4 NPs via a seed-mediated growth method.

Synthesis of SH-HPG-COOH dendrimers. NaH (0.01 mol, 60% in mineral oil) was added to a dioxane solution (10 ml) containing bis(2-hydroxyethyl) disulfide (120 μl) and mixed at 95 °C for 15 min. Then 4.2 ml of glycidol in 10 ml of dioxane was mixed dropwise under an argon atmosphere and stirred at 95 °C for 12 h.[23] After this reaction, the organic phase was removed, and the solid precipitate was dissolved in 10 ml of UPW. The polyglycerol solution was purified for 24 h by dialysis (molecular weight cutoff 3 K) and dried in a FD-2A vacuum freeze dryer (Biocool Experimental Equipment Co., Ltd, Beijing, China). The obtained disulfide-containing hyperbranched polyglycerol (HPG-S-S-HPG) (164 mg) was dissolved in 10 ml of UPW under an argon atmosphere. Then dithiothreitol (400 μl, 0.5 M) was added to the reaction mixture and reacted at 50 °C for 24 h. The yellow products were purified for 24 h by dialysis (molecular weight cutoff 3 K) and dried in a vacuum freeze dryer.

Synthesis of flower-like superparamagnetic Fe_3O_4@Au-HPG-Glc nanoprobes. The Fe_3O_4@Au NPs modified by HPG were modified with Glc to accelerate cellular uptake. In brief, 6 mg of HPG were added to a Fe_3O_4@Au NP solution (1 ml, 4 mg ml^{-1}) using ultrasound for 3 h. The obtained Fe_3O_4@Au-HPG was activated using 1.5 mg ml^{-1} *N*-hydroxysulfosuccinimide and 1-ethyl-3-[3-dimethylaminopropyl] carbodiimide hydrochloride in SBB 9 buffer (50 mM boric acid solution was adjusted to pH 9 using 0.4 M NaOH) for 30 min. The activated Fe_3O_4@Au-HPG NPs were collected by magnetic separation and subsequently reacted with Glc (1 mg) overnight at room temperature on a rotational mixer. The products were purified by magnetic separation. The concentration of Fe_3O_4@Au-HPG-Glc nanoprobes was determined by inductively coupled plasma (ICP)–atomic emission spectrometry.

Characterization

The morphologies of the Fe_3O_4 and Fe_3O_4@Au NPs were observed using transmission electron microscope (TEM) and high-resolution TEM (HRTEM) with a JEM-2100F instrument (JEOL, Tokyo, Japan). The ultraviolet (UV)–visible absorption spectra of Fe_3O_4@Au, Fe_3O_4@Au-HPG, Glc and Fe_3O_4@Au-HPG-Glc were measured using a Varian Cary 50 spectrophotometer (Varian Inc., Palo Alto, CA, USA). The Fourier transform infrared (FTIR) spectra of Fe_3O_4@Au, Fe_3O_4@Au-HPG and Fe_3O_4@Au-HPG-Glc were captured by a Nicolet 6700 spectrometer using KBr-supported pellets (Thermo Scientific, Waltham, MA, USA). Dynamic light scattering was measured with a NICOMP 380 ZLS ζ potential/particle sizer (PSS Nicomp, Santa Barbara, FL, USA). The magnetization loops of Fe_3O_4 and Fe_3O_4@Au-HPG-Glc were determined on an Ever Cool-II physical property measurement system with 9 Tesla magnets (Quantum Design, San Diego, CA, USA). The T_2 relaxation times of different concentrations of samples were obtained with a 1.4 T Bruker Minispec analyzer (nuclear magnetic resonance (NMR), MQ60, Karlsruhe, Germany). The various concentrations of nanoprobes (diluted with UPW) were shifted in sample tubes and remained constant, immersed in a 37 °C circulating water bath. The T_2 values corresponding to serial concentration (mM) plots for Fe_3O_4@Au-HPG-Glc NPs were obtained. The r_2 values (mM^{-1} s^{-1}) were obtained from the slopes of the optimum fits. MGC-803 cells were photographed with a microscope (NIKON TS100-F, Tokyo, Japan).

Cytotoxicity assay

The MGC-803 cells were incubated in 75-cm^2 cell culture flasks at 37 °C and 5% CO_2 and immersed in 20 ml of Dulbecco's Modified Eagle's Medium with penicillin (500 μl, 100 U ml^{-1}) and 10% (vol/vol) heat-inactivated fetal bovine serum. Then the toxicity of different concentrations of Fe_3O_4@Au-HPG and Fe_3O_4@Au-HPG-Glc were investigated using an MTT viability assay of MGC-803 cells.

Endocytosis of Fe_3O_4@Au-HPG-Glc NPs

MGC-803 cells (2×10^5 cells per well) were seeded in culture dishes overnight at a certain density and cultured in an incubator at 37 °C with 5% CO_2. Then the culture media were replaced with fresh media containing Fe_3O_4@Au-HPG-Glc NPs. After 24 h of culturing, the adherent cells were gently rinsed twice using phosphate-buffered saline (PBS) to remove noninternalized nanoprobes. Subsequently, the cells were trypsinized and concentrated into a pellet by centrifugation at 1300 r.p.m. for 5 min. Then the pelleted nanoprobes were dispersed in 2.5% glutaraldehyde overnight at 4 °C. Following conventional protocols, a slice of the cells was fixed on a copper net and stained. The distribution of synthesized nanoprobes adsorbed into cells was obtained by an 80 kV B-TEM (Tecnai G2 Spirit Biotwin, FEI, Tokyo, Japan). Untreated MGC-803 cells served as the control group.

In vitro cytoclasis of MGC-803 cells via mechanical rotation of Fe_3O_4@Au-HPG-Glc nanoprobes under an AMF

MGC-803 cells were incubated in three 6-cm-diameter culture dishes and allowed to adhere for 12 h. Subsequently, 5 ml of fresh media with the same concentrations of Fe_3O_4@Au-HPG and Fe_3O_4@Au-HPG-Glc (10 μl, 4 mg ml^{-1}) were added to each dish. The final concentrations of Fe_3O_4@Au-HPG and Fe_3O_4@Au-HPG-Glc interacting with MGC-803 cells were 8 μg ml^{-1}. The cells were washed three times using PBS solution to remove noninternalized targeted/nontargeted nanoprobes after 24 h of incubation. Simultaneously, fresh medium was added, and the culture dishes were placed directly on the center of a stirring platform for 5 min at 10-min intervals. MGC-803 cells were subjected three times to the mechanical rotation of targeted/nontargeted nanoprobes under an AMF and were monitored by fluorescence microscopy.

Establishment of the xenografted tumor models

Based on routine protocols advocated by the institutional committee for animal care and the National Ministry of Health, the animal experiments were carried out in accordance with the Ethics Committee of Shanghai Jiao Tong University. A transplanted tumor model of gastric cancer was prepared in the right flank skin of female nude mice via subcutaneous injection of 1×10^6 MGC-803 cells. After approximately 1 month, the formed solid tumors were harvested and cut into small fragments with edge lengths of approximately 0.2 cm. Then the healthy mice were anesthetized. An incision in the back right flank skin was made, and a small tumor lump was quickly pushed into the incision channel. Subsequently, the incision was sewn closed. After 4 additional weeks, the subcutaneously transplanted tumor models of gastric cancer were established. All surgical steps were completed in a sterile environment.

In vivo MRI

All MR *in vivo* imaging was carried out before and at fixed time points of 0, 4, 8, 12 and 24 h postinjection using a clinical 3.0 T Siemens Magnetom Trio medical MR system (Shanghai Sixth People's Hospital Radiology Department of MRI, Shanghai, China) with a customized small animal detection coil. The measurement parameters were: time to echo = 52 ms, repetition time = 2600 ms, field of

view = 1 × 1 cm^2, slice thickness = 2 mm, matrix = 320 × 256, NEX = 2, and acquisition time = 96 s. When collecting data at set time points, the tumor-burdened mice were anesthetized and placed in the coil. The corresponding T_2-weighted gray values were detectable with the clinical MRI software.

In vivo biodistribution

Female mice with subcutaneously transplanted tumors were injected with 100 μl of Fe_3O_4@Au-HPG and Fe_3O_4@Au-HPG-Glc (the mass ratio of the nanoprobes to total mouse body weight was 0.5 g kg^{-1}) via the tail vein. The mice were killed at 24 h postinjection. Then the main organs and tumors were harvested, weighed and digested using concentrated nitric acid overnight. Tumor and tissue fats were decomposed with perchloric acid under heating. The Fe and Au contents in the tumors and organs were obtained by ICP–atomic emission spectrometry and ICP–mass spectrometry.

In vivo magnetic therapy via mechanical rotation of Fe_3O_4@Au-HPG-Glc NPs under an AMF

To evaluate the therapeutic efficiency of the Fe_3O_4@Au-HPG-Glc nanoprobes, MGC-803 tumor-bearing mice were treated with 100 μl of either Fe_3O_4@Au-HPG or Fe_3O_4@Au-HPG-Glc. When the solid tumor volume was approximately 100 mm^3, five experiments (five mice per group) were prepared: (1) PBS (100 μl) with AMF; (2) Fe_3O_4@Au-HPG (0.5 g kg^{-1} of nanoprobes) without AMF; (3) Fe_3O_4@Au-HPG-Glc (0.5 g kg^{-1} of nanoprobes) without AMF; (4) Fe_3O_4@Au-HPG (0.5 g kg^{-1} of nanoprobes) with AMF; and (5) Fe_3O_4@Au-HPG-Glc (0.5 g kg^{-1} of nanoprobes) with AMF. For the therapy groups, a large rotating magnet (approximately 400 mT) was placed in the rearing cage after intratumoral injection to provide the AMF. The relevant optical images and tumor volume were recorded every 3 days. At day 12, the mice were killed, and the primary organs (for example, spleen, liver and kidney) of mice in the blank and experimental groups were collected and fixed with 4% paraformaldehyde overnight. Subsequently, these harvested tissues were sliced after paraffin embedding, fixed on a slide and stained using hematoxylin and eosin according to routine methods. Morphological characteristics and pathological changes were observed by microscopy.

Statistical analysis

All data were processed as the mean ± s.d. Statistical significance of the data was determined using the SPSS 18.0 software (IBM Co., Armonk, NY, USA) and based on Student's *t*-test. Differences of $P < 0.05$ and $P < 0.01$ were considered significant.

RESULTS AND DISCUSSION

Characterization of SH-HPG-COOH dendrimers

The synthesis of the HPG dendrimer is shown in Supplementary Figure S1. The structure of the HPG dendrimer was confirmed by the NMR spectra, including the ^1H (Supplementary Figure S2) and ^{13}C (Supplementary Figure S3) spectra. The ^1H NMR spectrum of HPG showed the characteristic proton signals of the -CH_2S- units of HPG at 2.7 p.p.m. Because hydroxyl groups will be used for anchoring biomolecules, succinic anhydride was used to convert the hydroxyl groups to carboxyl groups in order to promote bonding with the targeted molecules. The carboxyl groups in the HPG dendrimer were observed at 61 p.p.m. in the carbon spectrum (Supplementary Figure S3). The yellow monothiol-functionalized HPG solution was obtained by the reduction of disulfide bonds using dithiothreitol. Based on the ^1H NMR spectrum of HPG-S-S-HPG, the number-average (M_n) molecular weight was approximately 29 900 g mol^{-1} (Supplementary Figure S4). From the FTIR spectrum (Supplementary Figure S5), a wide absorption band at 3409 cm^{-1} can be attributed to the overlapping stretching vibrations of multiple alcoholic hydroxyl groups.[24] The peak at 1248 cm^{-1} was due to the C – O – C stretching vibrations on the HPG chain.[25] The characteristic peak at 1591 cm^{-1} confirmed the presence of COOH, which was consistent with the antisymmetric stretching vibration of carboxyl groups.[26] These results confirmed the formation of SH-HPG-COOH dendrimers.

Characterization of flower-like Fe_3O_4@Au and Fe_3O_4@Au-HPG-Glc NPs

The flower-like Fe_3O_4@Au NP structure was characterized by TEM and HRTEM. The nanoprobe composition was analyzed via energy-dispersive spectroscopy. Figure 2a shows that the flower-like Fe_3O_4 NPs (average diameter of approximately 60 nm) were uniform in shape and monodispersed. Figure 2b shows that the crystal spacing of the Fe_3O_4 NP was the same as a (111) lattice spacing (0.485 nm).[27] The clear crystal lattice indicated a highly crystalline nature of the flower-like Fe_3O_4 NPs. Figures 2c and d show that the flower-like Fe_3O_4 NPs were covered by an Au layer containing numerous

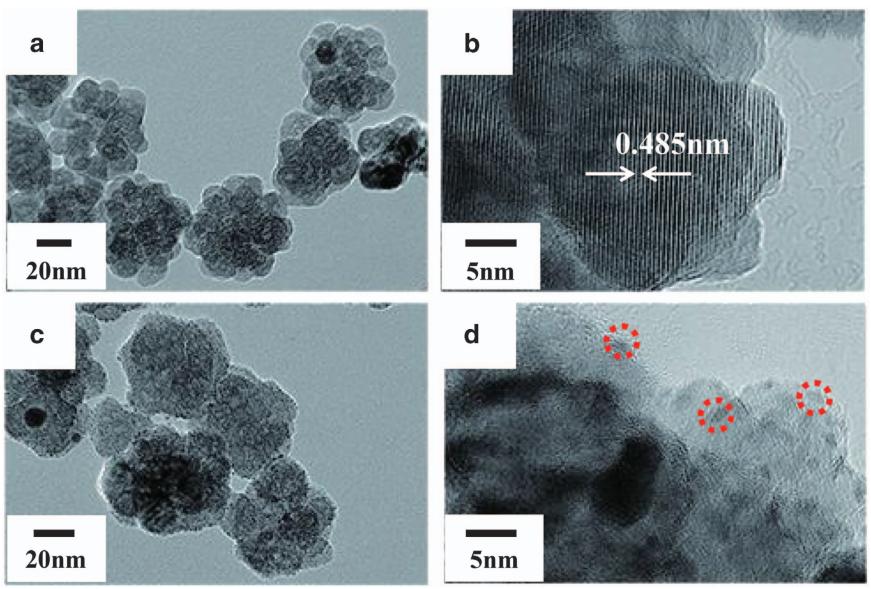

Figure 2 Representative TEM images of (**a**) Fe_3O_4 and (**c**) Fe_3O_4@Au; HRTEM images of (**b**) Fe_3O_4 and (**d**) Fe_3O_4@Au. Note that the red circles are labeled Au NPs on the surface of Fe_3O_4 NPs.

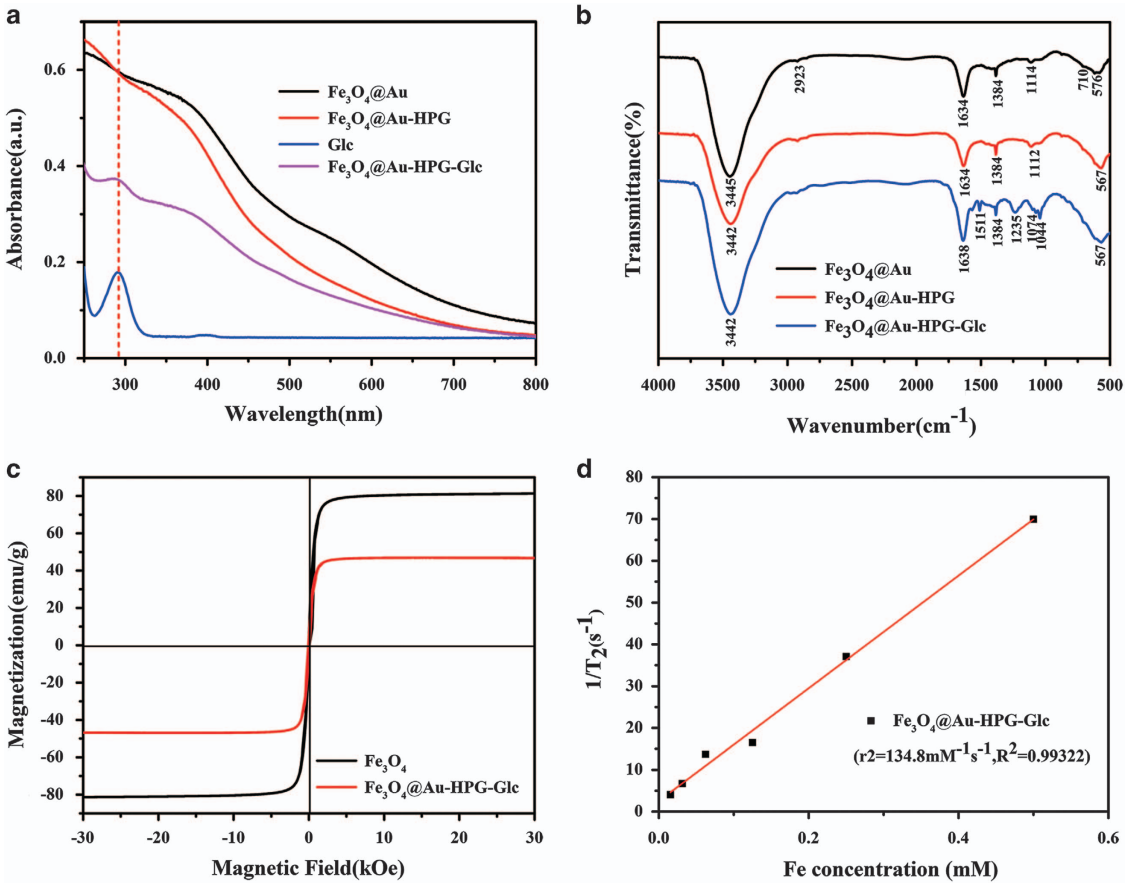

Figure 3 (**a**) UV–vis absorption of Fe_3O_4@Au (black curve), Fe_3O_4@Au-HPG (red curve), pure glucose (blue curve) and Fe_3O_4@Au-HPG-Glc (pink curve); (**b**) FTIR spectra of the Fe_3O_4@Au (black curve), Fe_3O_4@Au-HPG (red curve) and Fe_3O_4@Au-HPG-Glc nanoprobes (blue curve). (**c**) Magnetization loops of the Fe_3O_4 and Fe_3O_4@Au-PG-Glc nanoprobes, measured at 300 K. (**d**) Linear fitting of $1/T_2$ for Fe_3O_4@Au-HPG-Glc with Fe concentrations of 0.016, 0.032, 0.0625, 0.125, 0.25, 0.5 and 1 mM.

ultrasmall high-crystallinity Au NPs. The flower-like Fe_3O_4@Au composition was further verified by energy-dispersive spectroscopy (Supplementary Figure S6), revealing the existence of Au, Fe and O.

To enhance the colloidal stability of the obtained flower-like Fe_3O_4@Au NPs, the NPs were modified with HPG polymer, which contained a sufficient amount of sulfhydryl groups that facilitated the formation of gold–thiol bonds. The interaction with HPG dendrimers was confirmed by the UV–vis (Figure 3a) and FTIR spectra (Figure 3b). Fe_3O_4@Au-HPG-Glc was easily dispersed at high concentrations in various aqueous solutions, including PBS buffer solution (pH 7.4), cell media, UPW and deionized water (Supplementary Figure S7b). To improve cellular uptake, Glc was used as a target molecule and anchored to the surface of the Fe_3O_4@Au-HPG NPs. This improved the targeting ability of the NPs due to the overexpression of membrane Glc transporters in gastric cancer cells.[20] Furthermore, modifications with Glc potentially enhance the biocompatibility of NPs and reduce their cytotoxicity in clinical applications.[28]

The characteristic absorption peak at 280 nm in Figure 3a is representative of phenyl groups from Glc. Additionally, the peak in the UV–vis absorption curve of Fe_3O_4@Au-HPG-Glc also appeared at approximately 280 nm. This peak has a slight blueshift, and the absorption band appeared wider when compared with the peaks arising from pure Glc. These differences were attributed to the formation of an amide bond between the HPG dendrimer and Glc. The FTIR spectra of Fe_3O_4@Au-HPG NPs were also affected by the presence of Glc. From Figure 3b, four new absorption peaks were observed at 1044, 1074, 1235 and 1511 cm^{-1}. The 1511 and 1074 cm^{-1} peaks are assigned to the stretching vibrations of C=C bonds in the aromatic ring and C-OH bonds in Glc,[24] respectively. The peak at 1044 cm^{-1} is due to the symmetrical stretching vibration of C-O-C bonds.[25] The peaks approximately 1235 cm^{-1} are attributed to the stretching vibration of the C-N in secondary amides, which further confirmed successful covalent coupling between the HPG dendrimer and Glc.[29] After the modification by HPG, the Fe_3O_4@Au NPs still formed good dispersions due to the formation of gold–thiol bonds between rich hydroxyl/carboxyl functional groups and Au clusters (Supplementary Figure S7a). The as-prepared monodisperse flower-like Fe_3O_4@Au NPs can be easily dispersed into UPW and quickly separated by an external magnetic field within seconds. This excellent colloidal stability can enhance the application of Fe_3O_4@Au-HPG-Glc NPs for MRI and targeted therapy under AMFs. The hydrodynamic sizes of the Fe_3O_4@Au and Fe_3O_4@Au-HPG-Glc were 264 and 458 nm, respectively (Supplementary Figure S8), which are larger than the sizes determined by TEM. This difference was likely due to the aggregation of NPs in UPW, as reported in previous work.[30]

To explore the potential applications of flower-like Fe_3O_4@Au-HPG-Glc nanoprobes for MRI, magnetization loop and T_2 MR relaxometry measurements were carried out. The magnetization curves showed the superparamagnetic behavior of Fe_3O_4 and

Fe_3O_4@Au-PG-Glc nanoprobes. The saturation magnetizations were approximately 80.1 and 47.6 emu g^{-1} before and after modification (Figure 3c), respectively. The saturation magnetization was measured at 300 K with a field up to 3 T. Figure 3d shows that the r_2 relaxivity was 134.8 $mM^{-1}s^{-1}$, indicating that the synthesized flower-like Fe_3O_4@Au-HPG-Glc nanoprobes could be used as a T_2 contrast medium in MRI.[31] The cytotoxicity of flower-like Fe_3O_4@Au-HPG-Glc nanoprobes was measured via the MTT assay (Supplementary Figure S9). The cell survival rate was nearly unaffected by increasing nanoprobe concentrations. This result indicated that the HPG dendrimer layer on the surface of the Fe_3O_4@Au-HPG-Glc nanoprobes could enhance the biological compatibility and colloidal stability of the NPs to facilitate subsequent *in vivo* imaging and therapy.

In vitro cytoclasis of MGC-803 cells via mechanical rotation of Fe_3O_4@Au-HPG-Glc nanoprobes under an AMF

To evaluate the cellular localization of Fe_3O_4@Au-HPG-Glc nanoprobes, ultrastructural features of MGC-803 cells treated with nanoprobes under an AMF were observed using TEM. Figure 4a shows that, within observed black patches inside cell cytoplasm, nanoprobes were detected, which were formed via receptor-mediated endocytosis. Furthermore, the majority of internalized nanoprobes were located in lysosomes, suggesting an endocytotic mechanism (Figures 4b and c). Interestingly, the cytoplasm-distributed nanoprobes were encapsulated in bilayer membrane vesicles formed by grid proteins. Based on the TEM images, the majority of flower-like Fe_3O_4@Au-HPG-Glc nanoprobes were observed in the lysosomes of MGC-803. The Fe_3O_4@Au-HPG-Glc nanoprobes first interacted with receptors in cell membranes via a receptor-mediated method, leading to the formation of a pit coated with grid proteins. The vesicles were gradually formed through the invagination of the pit from the membrane. After the capsule depolymerization of the vesicles, the vesicles were integrated with lysosomes. The phagotrophic nanoprobes were hydrolyzed by lysosomal enzymes. Enzymatic hydrolysates remained distributed in the cytoplasm. Under an AMF, all flower-like nanoprobes distributed in these sites were rotated, which resulted in the mechanical destruction of tumor cells via cell membrane damage, organelle damage and cell disintegration. Via these external magnetic field effects, the partial flower-like nanoprobes thoroughly damaged cell nuclei, reducing drug resistance. The special rotating property of the flower-like Fe_3O_4@Au-HPG-Glc nanoprobes suggested the feasibility of using these nanoprobes as 'nano-turbine blades' under an AMF.

Figures 5 and 6 show the morphology at different magnifications of MGC-803 cells after treatment with Fe_3O_4@Au-HPG-Glc nanoprobes under an AMF. The cells were stretched (Figure 6a), and pinholes appeared in the cell membranes (Figure 6b and 6d). Some cells disintegrated Figure 6c, and the 'nano-turbine blade' may have destroyed the tumor cells with the assistance of an AMF. This powerful physical therapy will likely reduce the drug resistance commonly encountered in malignant tumor therapy. Interestingly, the residual enzymatic hydrolysate distributed in the cytoplasm can still have a key role in damaging other organelles to provide novel pathways for tumor treatment.

In vivo MRI

To verify the effectiveness of Fe_3O_4-based nanoprobes as a T_2 contrast agent, nontargeted Fe_3O_4@Au-HPG and targeted Fe_3O_4@Au-HPG-Glc were intravenously injected into mice for MRI. Compared with the nontargeted Fe_3O_4@Au-HPG nanoprobes, the targeted Fe_3O_4@Au-HPG-Glc nanoprobes exhibited prolonged retention in the tumor boundaries due to enhanced cellular endocytosis and accumulation in the tumor site via binding with corresponding ligands.[32] T_2-weighted MR images (Figure 7a) in the tumor site were acquired before injection and at 0, 4, 8, 12 and 24 h postinjection. Compared with the MR signal values before injection, the MR signal value of mice injected with nontargeted Fe_3O_4@Au-HPG had a decreasing trend up to 8 h and showed an evident increase after 12 h, indicating that the endocytotic nanoprobes in the tumor were further metabolized by the reticuloendothelial system of the tumor cells.[30] The MR signal values in mice tumors treated with Fe_3O_4@Au-HPG-Glc nanoprobes showed a decreasing trend before 12 h and presented a slight increase at 24 h. This effect may be attributed to the Glc-mediated targeting effect acting as a synergistic motivator to enhance the uptake of Fe_3O_4@Au-HPG-Glc nanoprobes. The time-dependent MR signal intensities and relative T_2-signal changes ($\Delta T_2/T_2$) of the tumors were quantitatively analyzed. As shown in Figures 7b and c, the tumor signal intensity of the control group reached a minimum value of 1331.96 at 8 h postinjection due to the passive enhanced permeability and retention effect. However, the tumor signal intensity of the experimental group decreased remarkably from 1901.07 (0 h) to 1190.27 at 12 h postinjection due to passive and active targeting. Additionally, the distribution of the Fe_3O_4@Au-HPG-Glc nanoprobes in the tumors was more uniform than that of the nontargeted NPs. As expected, cellular internalization was improved to some extent by the special

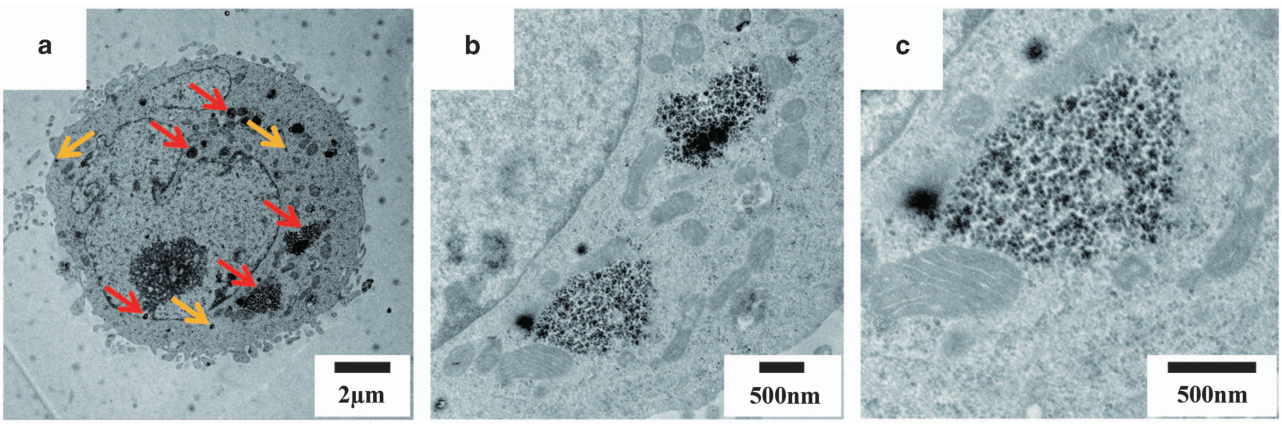

Figure 4 TEM images of MGC-803 cells treated with Fe_3O_4@Au-HPG-Glc nanoprobes was observed under low power (**a**), intermediate magnification in the selected area (**b**) and high magnification in the selected area (**c**). Note that the red arrows indicate the nanoprobes in cytoplasm of the MGC-803 cells, and the yellow arrows indicate nanoprobe dispersions as secretions being excluded by the MGC-803 cells.

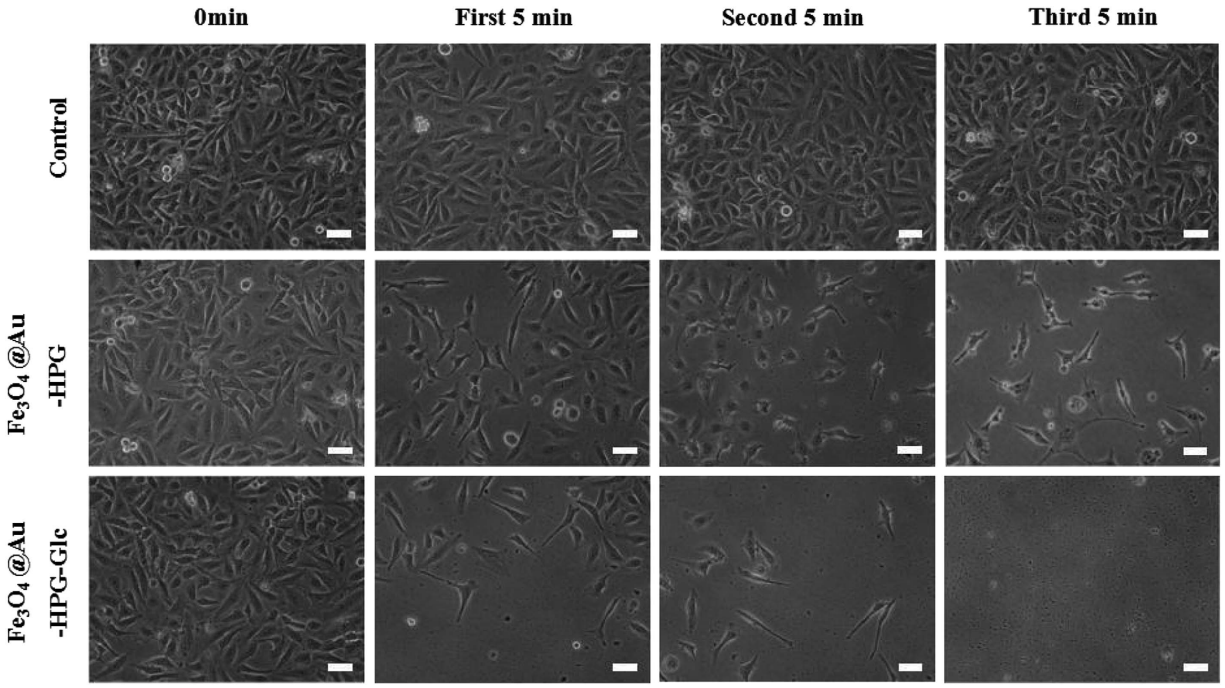

Figure 5 *In vitro* physical therapy. The microscope images at ×20 magnification of cells treated with Fe_3O_4@Au-HPG and Fe_3O_4@Au-HPG-Glc under alternating magnetic field and microscope photos of cells under alternating magnetic field (experimental group), scale bar: 100 μm.

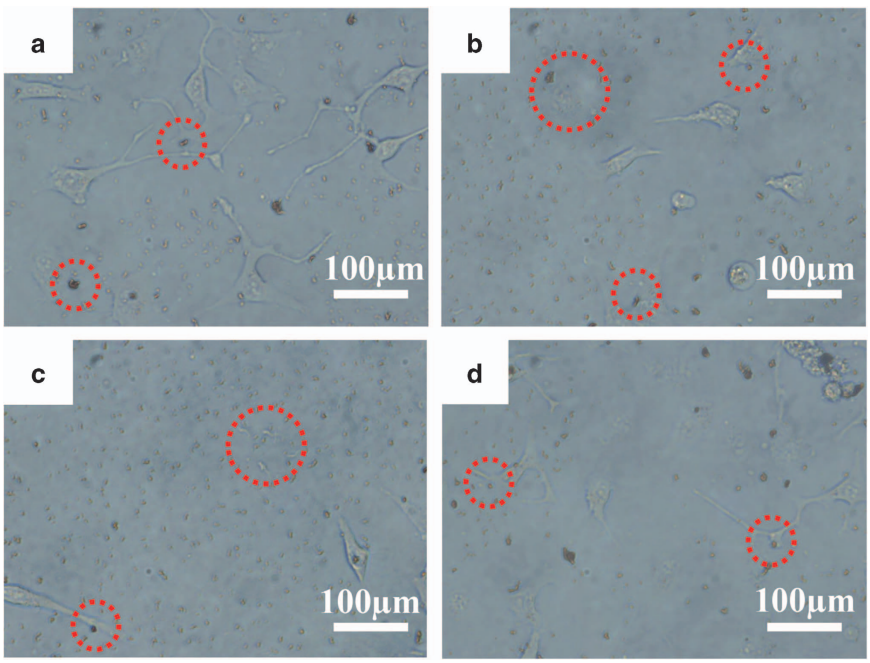

Figure 6 *In vitro* physical therapy. The representative microscope images at × 40 magnification of cells that had interacted with Fe_3O_4@Au-HPG-Glc nanoprobes under alternating magnetic field. The cellular response to AMF stimulation mainly include stretching deformation (**a**), cell membrane perforation (**b**, **d**), and cell disruption (**c**). Note that the red circles were labeled nanoprobes in the cells' outer edge and inside region.

targeting effect. The results indicated that the synthesized Fe_3O_4@Au-HPG-Glc nanoprobes showed considerable potential as a prolonged tumor-targeted T_2 contrast agent for clinical applications.

In vivo biodistribution of Fe_3O_4@Au-HPG-Glc nanoprobes

To evaluate the targeting efficiency and biodistribution behavior of Fe_3O_4@Au-HPG-Glc nanoprobes, the uptake of Fe and Au in the tumors and major organs (for example, liver, kidneys and spleen) at 24 h postinjection were quantitatively analyzed using ICP–atomic emission spectrometry and ICP–mass spectrometry, respectively. The distribution of Fe (Figure 8a) in the tumors and major organs was fairly consistent compared with that of Au (Figure 8b). We found that Fe and Au were distributed in the liver (72.35 μg Fe and 71.83 ng Au per gram liver tissue), kidneys (65.16 μg Fe and 93.55 ng Au per gram kidney tissue) and spleen (17.11 μg Fe and 39.17 ng Au per gram spleen tissue) at 24 h postinjection. Although a few Fe_3O_4@Au-HPG-

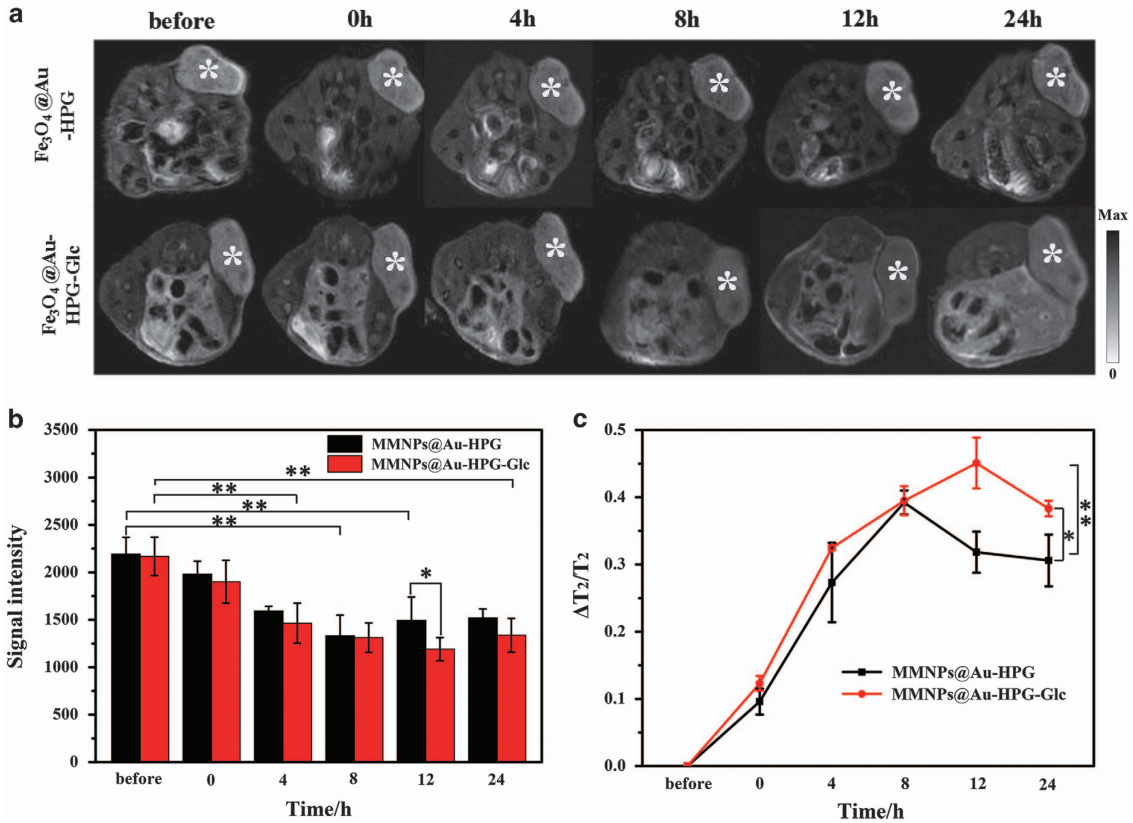

Figure 7 *In vivo* MRI. (**a**) The T_2-weighted MR images of the mice bearing MGC-803 tumor before and after injection of the nontargeted Fe_3O_4@Au-HPG or targeted Fe_3O_4@Au-HPG-Glc; (**b**) the signal intensity of MRI in tumor sites; (**c**) the relative T_2-signal change ($\Delta T_2/T_2$) in tumor sites before and after injection. $^*P<0.05$, $^{**}P<0.01$.

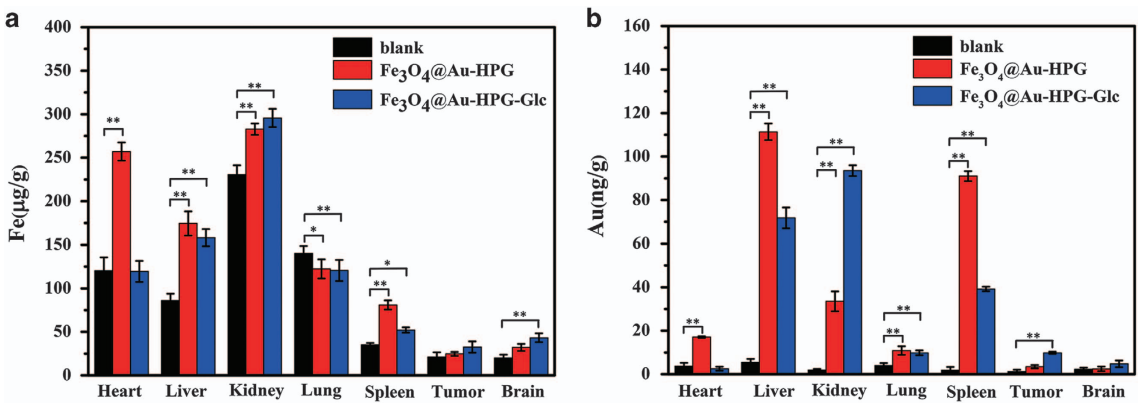

Figure 8 *In vivo* biodistribution of (**a**) Fe and (**b**) Au in tumors and major organ tissue of the tumor-bearing mice 24 h after injection of the Fe_3O_4@Au-HPG and Fe_3O_4@Au-HPG-Glc, compared with the blank group. $^*P<0.05$, $^{**}P<0.01$.

Glc nanoprobes were detected in these tissues, there was no toxicity or side effects in the absence of an AMF. The targeted-Fe_3O_4@Au-HPG-Glc nanoprobes accumulated in the tumor site to approximately 65%, which was significantly higher than that of the nontargeted Fe_3O_4@Au-HPG nanoprobes, demonstrating the effectiveness of these NPs for MRI-guided tumor therapy.

In vivo physical therapeutic efficacy of Fe_3O_4@Au-HPG-Glc NPs

To evaluate the *in vivo* physical therapeutic efficacy of Fe_3O_4@Au-HPG-Glc nanoprobes, changes in tumor volumes were recorded using Vernier calipers for 12 days (Figure 9a). Mice tumor sites were treated with PBS, Fe_3O_4@Au-HPG nanoprobes or Fe_3O_4@Au-HPG-Glc nanoprobes in the presence and absence of an AMF for 1 h after 8, 24 and 36 h postinjection, respectively. Figure 9b shows that the tumor growth of the blank group (PBS) under an AMF was much faster than the other experimental groups. Compared with the blank group, the inhibition of tumor growth in mice treated with Fe_3O_4@Au-HPG-Glc/AMF was up to ~47.3% on the twelfth day, indicating a remarkable efficacy. The tumor growth of MGC-803-bearing mice treated with Fe_3O_4@Au-HPG/AMF was ~25.7%. However, the inhibition of tumor growth of mice treated with Fe_3O_4@Au-HPG nanoprobes in the absence of AMF was nearly negligible and that of Fe_3O_4@Au-HPG-Glc

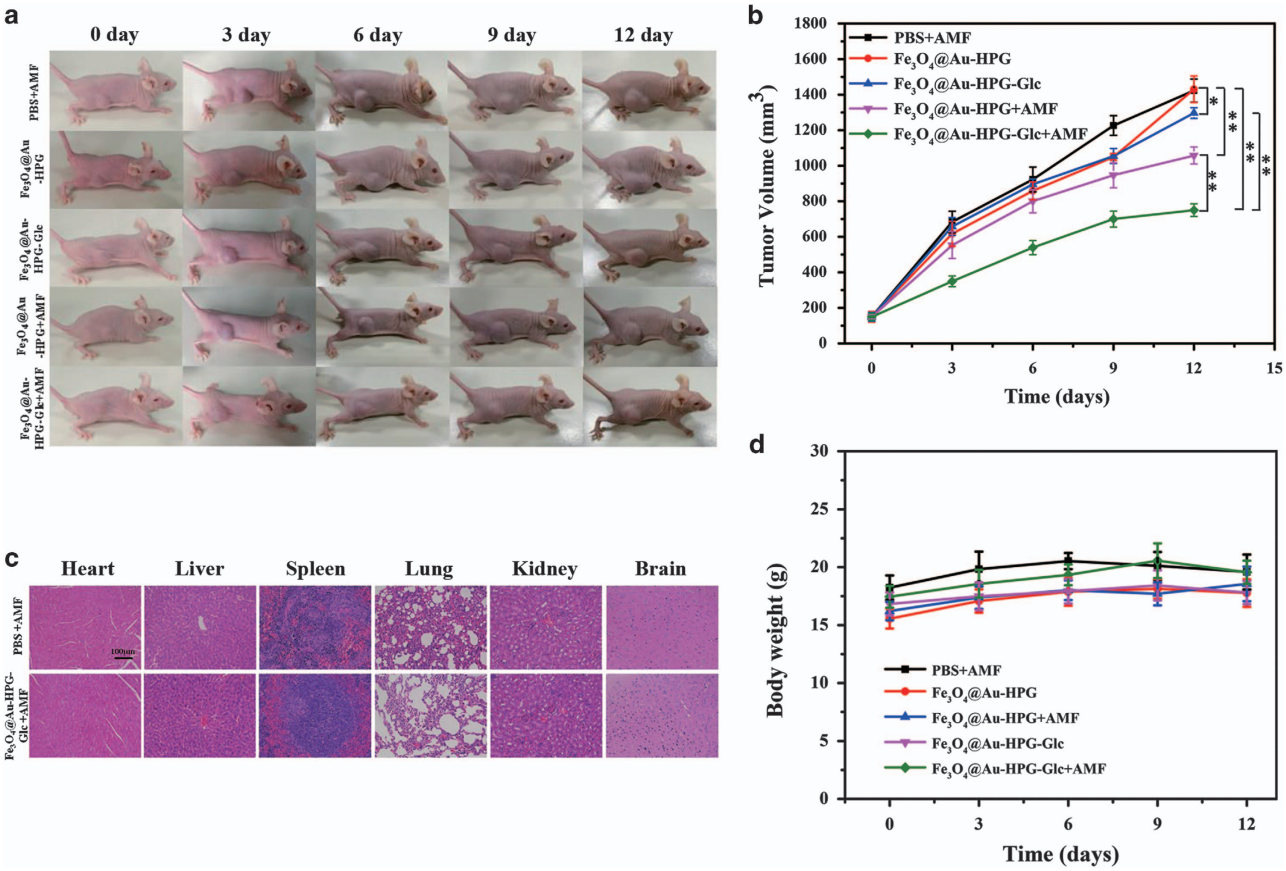

Figure 9 *In vivo* physical therapy. (**a**) The time-dependent optical images for MRI-guided physical destruction of tumor; (**b**) growth curves of tumor volume of mice interacted with different kinds of nanoprobes for 18 days; (**c**) H&E staining of major organs of mice treated with PBS (blank group) and Fe_3O_4@Au-HPG-Glc nanoprobes (experimental group) under alternating magnetic field (scale bar = 100 μm); (**d**) changing curves of mice body weight after treatment using different methods. $^*P<0.05$, $^{**}P<0.01$.

nanoprobes without an AMF was approximately 8.9%. Additionally, as shown in Supplementary Figure S10, at day 12, many more damaged cells were observed in the Fe_3O_4@Au-HPG-Glc+AMF group and no obvious damaged tumor cells were observed in the PBS+AMF group. Fe_3O_4@Au-HPG-Glc nanoprobes stimulated by an AMF had remarkable efficacy for MRI-guided physical therapy due to the targeted uptake by tumor cells and tumor cell disruption. To evaluate the potential toxicity of flower-like Fe_3O_4@Au-HPG-Glc nanoprobes, variations in mice weight were measured using a visual indicator. Figure 9d shows no evident changes in mice weight in the blank and experimental groups. At day 12, mice were killed, and isolated organs were embedded in paraffin and sectioned. Using hematoxylin and eosin staining, the obtained tissue sections were examined using microscopy. Figure 9c shows that the organ tissues of the experimental group had no evident pathological changes or other anomalies when compared with the blank group. Histopathological examinations after treatment under an AMF further confirmed that the Fe_3O_4@Au-HPG-Glc nanoprobes were safe and had no evident toxicity and side effects *in vivo*. Considering the low retention of Fe_3O_4@Au-HPG-Glc nanoprobes in the spleen, liver and kidneys after 24 h injection, no distinct long-cycle side effects were observed after 12 days *in vivo* therapy.

CONCLUSIONS

In summary, we developed a novel flower-like targeting Fe_3O_4@Au-HPG-Glc nanoprobe for effective MRI and enhanced gastric tumor therapy. The nanoprobes integrated dendrimers, targeting molecules and unique flower-like Fe_3O_4@Au NPs into a versatile all-in-one nanoplatform. Under an AMF, the biodegradable flower-like Fe_3O_4@Au nanoprobes can be rotated owing to axial dissymmetry. This special behavior promoted the mechanical destruction of tumor cells (for example, cell membrane damage, organelle damage and nuclear damage), which could potentially reduce malignant tumor therapy drug resistance. Simultaneously, the tumor lesion and boundary can be precisely diagnosed using real-time MRI. Based on MRI, the Fe_3O_4@Au-HPG-Glc nanoprobes were targeted to tumor sites under an AMF. The synthesized Fe_3O_4@Au-HPG-Glc nanoprobes exhibited good biocompatibility, colloidal stability, specific active targeting and nonimmunogenicity. Only under an AMF for 15 min, cultured MGC-803 cells were completely destroyed. Furthermore, the inhibition of tumor growth in mice treated with Fe_3O_4@Au-HPG-Glc nanoprobes can reach up to ~47.3% by the twelfth day. The special flower-like structure of Fe_3O_4@Au-HPG-Glc nanoprobes may be used for the repeated treatment of tumors under AMFs. These nanoprobes are superior to traditional nanoprobes with spherical structures. The application of flower-like structure of Fe_3O_4@Au-HPG-Glc nanoprobes for the targeted therapy of gastric tumor provides a new pathway for resolving drug resistance issues of current cancer therapies.

CONFLICT OF INTEREST

The authors declare no conflict of interest.

ACKNOWLEDGEMENTS

Financial support was provided from the National Natural Science Foundation of China (No. 81671737, 81225010 and 91634108), the 863 High-Tech project of China (2014AA020701) and the 973 Project (2015CB931802).

Author contributions: All authors contributed to data analysis and the writing of this manuscript; all authors reviewed and approved the final version of this manuscript.

1 Lee, D. E., Koo, H., Sun, I. C., Ryu, J. H., Kim, K. & Kwon, I. C. Multifunctional nanoparticles for multimodal imaging and theragnosis. *Chem. Soc. Rev.* **41**, 2656–2672 (2012).
2 Chen, Q., Li, K. A., Wen, S. H., Liu, H., Peng, C., Cai, H. D., Shen, M. W., Zhang, G. X. & Shi, X. Y. Targeted CT/MR dual mode imaging of tumors using multifunctional dendrimer-entrapped gold nanoparticles. *Biomaterials* **34**, 5200–5209 (2013).
3 Yang, H., Zhuang, Y. M., Sun, Y., Dai, A. T., Shi, X. Y., Wu, D. M., Li, F. Y., Hu, H. & Yang, S. P. Targeted dual-contrast T_1-and T_2-weighted magnetic resonance imaging of tumors using multifunctional gadolinium-labeled superparamagnetic iron oxide nanoparticles. *Biomaterials* **32**, 4584–4593 (2011).
4 Debouttière, P. J., Roux, S., Vocanson, F., Billotey, C., Beuf, O., Favre-Réguillon, A., Lin, Y., Pellet-Rostaing, S., Lamartine, R., Perriat, P. & Tillement, O. Design of gold nanoparticles for magnetic resonance imaging. *Adv. Funct. Mater.* **16**, 2330–2339 (2006).
5 Roy, K., Kanwar, R. K. & Kanwar, J. R. LNA aptamer based multi-modal, Fe_3O_4-saturated lactoferrin (Fe_3O_4-bLf) nanocarriers for triple positive (EpCAM, CD133, CD44) colon tumor targeting and NIR, MRI and CT imaging. *Biomaterials* **71**, 84–99 (2015).
6 Wang, Y. & Gu, H. C. Core–shell-type magnetic mesoporous silica nanocomposites for bioimaging and therapeutic agent delivery. *Adv. Mater.* **27**, 576–585 (2015).
7 Yin, T., Huang, P., Gao, G., Shapter, J. G., Shen, Y. L., Sun, R. J., Yue, C. X., Zhang, C. L., Liu, Y. L., Zhou, S. & Cui, D. X. Superparamagnetic Fe_3O_4-PEG_{2K}-FA@Ce6 nanoprobes for in vivo dual-mode imaging and targeted photodynamic therapy. *Sci. Rep.* **6**, 36187 (2016).
8 Wang, T., Wang, X. R., LaMontagne, D., Wang, Z. L., Wang, Z. W. & Cao, Y. C. Shape-controlled synthesis of colloidal superparticles from nanocubes. *J. Am. Chem. Soc.* **134**, 18225–18228 (2012).
9 Qiao, Z. & Shi, X. Y. Dendrimer-based molecular imaging contrast agents. *Prog. Polym. Sci.* **44**, 1–27 (2015).
10 Zheng, Y., Fu, F. F., Zhang, M. E., Shen, M. W., Zhu, M. F. & Shi, X. Y. Multifunctional dendrimers modified with alpha-tocopheryl succinate for targeted cancer therapy. *Med. Chem. Commun.* **5**, 879–885 (2014).
11 Zhu, J. Y., Fu, F. F., Xiong, Z. J., Shen, M. W. & Shi, X. Y. Dendrimer-entrapped gold nanoparticles modified with RGD peptide and alpha-tocopheryl succinate enable targeted theranostics of cancer cells. *Colloid Surf. B* **133**, 36–42 (2015).
12 Peng, C., Li, K. A., Cao, X. Y., Xiao, T. T., Hou, W. X., Zheng, L. F., Guo, R., Shen, M. W., Zhang, G. X. & Shi, X. Y. Facile formation of dendrimer-stabilized gold nanoparticles modified with diatrizoic acid for enhanced computed tomography imaging applications. *Nanoscale* **4**, 6768–6778 (2012).
13 Liu, H., Wang, H., Xu, Y. H., Guo, R., Wen, S. H., Huang, Y. P., Liu, W. N., Shen, M. W., Zhao, J. L., Zhang, G. X. & Shi, X. Y. Lactobionic acid-modified dendrimer-entrapped gold nanoparticles for targeted computed tomography imaging of human hepatocellular carcinoma. *ACS Appl. Mater. Interfaces* **6**, 6944–6953 (2014).
14 Liu, H., Wang, H., Xu, Y. H., Shen, M. W., Zhao, J. L., Zhang, G. X. & Shi, X. Y. Synthesis of PEGylated low generation dendrimer-entrapped gold nanoparticles for CT imaging applications. *Nanoscale* **6**, 4521–4526 (2014).
15 Alexis, F., Pridgen, E., Molnar, L. K. & Farokhzad, O. C. Factors affecting the clearance and biosidtribution of polymeric nanoparticles. *Mol. Pharm.* **5**, 505–515 (2008).
16 Liang, S. J., Li, C., Zhang, C. L., Chen, Y. S., Xu, L., Bao, C. C., Wang, X. Y., Liu, G., Zhang, F. C. & Cui, D. X. CD44v6 monoclonal antibody-conjugated gold nanostars for targeted photoacoustic imaging and plasmonic photothermal therapy of gastric cancer stem-like cells. *Theranostics* **5**, 970–984 (2015).
17 Elghanian, R., Storhoff, J. J., Mucic, R. C., Letsinger, R. L. & Mirkin, C. A. Selective colorimetric detection of polynucleotides based on the distance-dependent optical properties of gold nanoparticles. *Science* **277**, 1078–1081 (1997).
18 Sur, I., Cam, D., Kahraman, M., Baysal, A. & Culha, M. Interaction of multi-functional silver nanoparticles with living cells. *Nanotechnology* **21**, 175104 (2010).
19 Kong, T., Zeng, J., Wang, X. P., Yang, X. Y., Yang, J., McQuarrie, S., McEwan, A., Roa, W., Chen, J. & Xing, J. Z. Enhancement of radiation cytotoxicity in breast-cancer cells by localized attachment of gold nanoclusters. *Small* **4**, 1537–1543 (2008).
20 Han, J. S., Zhang, J. J., Yang, M., Cui, D. X. & Fuente, J. M. Glucose-functionalized Au nanoprisms for optoacoustic imaging and near-infrared photothermal therapy. *Nanoscale* **8**, 492–499 (2016).
21 Li, Z. W., Yin, S. N., Cheng, L., Yang, K., Li, Y. G. & Liu, Z. Magnetic targeting enhanced theranostic strategy based on multimodal imaging for selective ablation of cancer. *Adv. Funct. Mater.* **24**, 2312–2321 (2014).
22 Zhang, C. L., Li, C., Liu, Y. L., Zhang, J. P., Bao, C. C., Liang, S. J., Wang, Q., Yang, Y., Fu, H. L., Wang, K. & Cui, D. X. Gold nanoclusters-based nanoprobes for simultaneous fluorescence imaging and targeted photodynamic therapy with superior penetration and retention behavior in tumors. *Adv. Funct. Mater.* **25**, 1314–1325 (2015).
23 Yeh, P. J., Kainthan, R. K., Zou, Y. Q., Chiao, M. & Kizhakkedathu, J. N. Self-assembled monothiol-terminated hyperbranched polyglycerols on a gold surface: a comparative study on the structure, morphology, and protein adsorption characteristics with linear poly(ethylene glycol)s. *Langmuir* **24**, 4907–4916 (2008).
24 Lim, S. F., Zheng, Y. M., Zou, S. W. & Chen, J. P. Characterization of copper adsorption onto an alginate encapsulated magnetic sorbent by a combined FT-IR, XPS, and mathematical modeling study. *Environ. Sci. Technol.* **42**, 2551–2556 (2008).
25 Cheng, C. H., Lehmann, J., Thies, J. E., Burton, S. D. & Engelhard, M. H. Oxidation of black carbon by biotic and abiotic processes. *Org. Geochem.* **37**, 1477–1488 (2006).
26 Sun, P., Zhang, H. Y., Liu, C., Fang, J., Wang, M., Chen, J., Zhang, J. P., Mao, C. B. & Xu, S. K. Preparation and characterization of Fe_3O_4/CdTe magnetic/fluorescent nanocomposites and their applications in immuno-labeling and fluorescent imaging of cancer cells. *Langmuir* **26**, 1278–1284 (2010).
27 Gao, G., Huang, P., Zhang, Y. X., Wang, K., Qin, W. & Cui, D. X. Gram scale synthesis of superparamagnetic Fe_3O_4 nanoparticles and fluid via a facile solvothermal route. *Cryst. Eng. Commun.* **13**, 1782–1785 (2011).
28 Barrientos, A. G., Fuente, J. M., Rojas, T. C., Fernandez, A. & Penades, S. Gold glyconanoparticles: synthetic polyvalent ligands mimicking glycocalyx-like surfaces as tools for glycobiological studies. *Chem. Eur. J.* **9**, 1909–1921 (2003).
29 Asher, S. A., Ianoul, A., Mix, G., Boyden, M. N., Karnoup, A., Diem, M. & Schweitzer-Stenner, R. Dihedral ψ angle dependence of the amide III vibration: a uniquely sensitive UV resonance raman secondary structural probe. *J. Am. Chem. Soc.* **123**, 11775–11781 (2001).
30 Cai, H. D., Li, K. A., Li, J. C., Wen, S. H., Chen, Q., Shen, M. W., Zheng, L. F., Zhang, G. X. & Shi, X. Y. Dendrimer-assisted formation of Fe_3O_4/Au nanocomposite particles for targeted dual mode CT/MR imaging of tumors. *Small* **11**, 4584–4593 (2015).
31 Kim, B. H., Lee, N., Kim, H., An, K., Park, Y. I., Choi, Y., Shin, K., Lee, Y., Kwon, G. S., Na, H. B., Park, J. G., Ahn, T. Y., Kim, Y. W., Moon, W. K., Choi, S. H. & Hyeon, T. Large-scale synthesis of uniform and extremely small-sized iron oxide nanoparticles for high-resolution T1 magnetic resonance imaging contrast agents. *J. Am. Chem. Soc.* **133**, 12624–12631 (2011).
32 Varallyay, P., Nesbit, G., Muldoon, L. L., Nixon, R. R., Delashaw, J., Cohen, J. I., Petrillo, A., Rink, D. & Neuwelt, E. A. Comparison of two superparamagnetic viral-sized iron oxide particles ferumoxides and ferumoxtran-10 with a gadolinium chelate in imaging intracranial tumors. *Am. J. Neuroradiol.* **23**, 510–519 (2002).

Supplementary Information accompanies the paper on the NPG Asia Materials website (http://www.nature.com/am)